J Electroceram (2006) 17:267–275
DOI 10.1007/s10832-006-6710-9

Device applications of transparent oxide semiconductors: Excitonic blue LED and transparent flexible TFT

Toshio Kamiya · Hidenori Hiramatsu · Kenji Nomura · Hideo Hosono

Received: 30 July 2005 / Revised: 30 July 2005 / Accepted: 16 December 2005

Abstract Recent progress in oxide-based transparent optoelectronic devices is reviewed. It is important to understand electronic structures inherent to oxides in order to develop new materials and to find suitable device applications that oxide materials can have distinct advantages over conventional semiconductors. Two new transparent oxide semiconductors, (i) *p*-type layered oxychalcogenides LaCuO*Ch* (*Ch* = chalcogen), and (ii) large-mobility amorphous oxide semiconductors (AOSs), are taken as examples. Their peculiar properties are discussed in comparison with conventional semiconductors based on consideration of electronic structures. Two associated devices, an excitonic light-emitting diode using LaCuO*Ch* and transparent flexible thin film transistors using AOSs, are also shown.

Keywords Transparent oxide semiconductor · Optoelectronic devices · Light-emitting diode · Thin film transistor · Electronic structure · Materials design

T. Kamiya (✉) · H. Hosono
Materials and Structures Laboratory, Tokyo Institute of Technology, Yokohama 226-8503, Japan
e-mail: tkamiya@msl.titech.ac.jp

T. Kamiya · H. Hiramatsu · K. Nomura · H. Hosono
ERATO-SORST, Japan Science and Technology Agency, in Frontier Collaborative Research Center, Tokyo Institute of Technology, Yokohama 226-8503, Japan

H. Hosono
Frontier Collaborative Research Center, Tokyo Institute of Technology, Yokohama 226-8503, Japan

1 Introduction

In the last decade, there has been large progress in oxide electronics, which has been driven by finding of the first *p*-type transparent oxide semiconductor (TOS) $CuAlO_2$ [1], extensive development research on ZnO [2–4], fever of strong electron correlation systems [5] and so on. Among oxide semiconductors, TOSs are of special interest both in solid-state physics and technology because optical transparency and good controllability of electrical conductivity coexist in TOSs although it is in general believed that wider bandgap materials are more difficult to attain good electrical properties. However, it is a misconception as demonstrated by recent works: electronic activities can indeed be rendered in many wide bandgap materials if we properly understand electronic structures and find a suitable way to design their chemical compositions and structures [6, 7].

In this paper, we first review recent progress in oxide electronics together with our strategy for developing the future oxide-based devices. Then two examples of new TOSs are introduced, (i) *p*-type layered oxychalcogenides *Ln*CuO*Ch* (*Ln* = lanthanides, *Ch* = chalcogen), and (ii) large-mobility amorphous oxide semiconductors (AOSs) in an In–Ga-Zn-O system (a-IGZO), along with our material exploration approach. Associated device applications, an excitonic light-emitting diode (LED) using LaCuO*Ch* and transparent flexible thin film transistors (TFTs) using AOSs, will also be shown.

2 Recent progress and issues in oxide-based optoelectronic devices (see refs. [6–9] for more reviews)

In these years, many oxide-based optoelectronic devices have been developed. The first ultraviolet (UV) LED using an oxide for a light-emitting layer was reported in 2000 [10, 11].

It uses a *p/n* junction structure composed of ZnO for light-emitting *n*-layer and $SrCu_2O_2$ for *p*-layer. Fully transparent high-performance TFTs were fabricated using single-crystalline films of $InGaO_3(ZnO)_5$ for channels and exhibited large field-effect mobilities of ∼80 cm^2/Vs at room temperature [12]. However, these devices have issues to be solved if we intend to apply them to practical devices, because similar devices are already in market using conventional semiconductors such as GaN and Si with better performances. It would be difficult for the oxide-based devices to compete with the conventional devices if their targets are the same because electronic structures and opto-electronic properties of oxide semiconductors are very different from those of the conventional covalent semiconductors. Therefore, we have to seek new opportunity and applications that only oxides can realize and/or oxides can find a clear advantage over the conventional devices.

Here, we like to propose some approaches. An idea is to get into deep UV region because wide bandgap is an inherent advantage of oxides. Ga_2O_3 is a unique material that has reasonably good electrical conductivity and high transmittance down to very short wavelengths ∼257 nm [13, 14]. We confirmed operation of TFTs using Ga_2O_3 for channel [15] and expect that it will be used for photo-sensors by combining with DUV optical fibers [16, 17]. This possibility will develop novel tools in chemical biology for detecting e.g. DNA and proteins because these molecules have intense absorption in DUV region. Another approach is to utilize natural nanostructures embedded in crystal structure of ionic semiconductors. $12CaO{\cdot}7Al_2O_3$, so-called C12A7, has subnanometer-sized cages in its crystal structure. These cages can accommodate active anions such as O^- [18] and H^- [19], and these anions exhibit new functions such as strong oxidation power and UV-induced persistent insulator—conductor conversion. It is also possible to introduce electrons instead of these anions [20], which exhibits electrical conductivities up to 100 S/cm (recent work suggests the largest conductivity runs up to >500 S/cm). It has a small workfunciton, and therefore it works as a good electron emitter [21, 22]. Operation of field-effect transistors is also confirmed [23], which provides a way for developing mesoscopic electronic devices utilizing the subnanometer-sized cages and the clathrated anions for quantum dots and charging islands [24, 25].

It should be noted that the most important feature of oxides would be that oxide-based devices operate even if they are formed at room temperature although covalent semiconductors such as amorphous silicon and poly-/microcrystalline silicon need to be passivated with hydrogen [26, 27]. *P/n* junction rectifiers fabricated using AOSs operate with good rectifying characteristics even if they are fabricated at room temperature [28, 29]. It is also reported that polycrystalline ZnO TFTs fabricated at room temperature work with reasonable field effect mobilities of ∼27 cm^2/Vs [30, 31]. The difference from silicon will be discussed in Section 4 with a relevant application of AOSs, flexible transparent TFTs.

As for LED, the first oxide-based UV LEDs were fabricated using a *p/n* junction structure in which ZnO was used for light-emitting n-layer and $SrCu_2O_2$ for non-radiative *p*-layer as explained above. In such a structure, holes must be injected to the n-layer to emit light by recombining with the electrons. However, as hole mobility is usually much lower than electron mobility in oxides because hole transport paths are mainly made of rather localized O 2p orbitals [7, 32]. Therefore, a large portion of electric energy is dissipated by electrons injected to the non-radiative *p*-layer. A way to improve light-emission efficiency in oxide-based LEDs is to employ a light-emitting *p*-layer. A more efficient way is to employ a double heterojunction structure in which both electrons and holes are confined in the light-emitting i-layer (intrinsic layer) by the potential barriers made by the p/i and i/n heterointerfaces (blocking layers). In addition, high-conductivity n^+- and p^+-layers are necessary to reduce series resistance by improving semiconductor—metal contacts.

To fabricate such a device, we needed to find new materials because we did not have light-emitting *p*-type materials in TOSs and materials for the blocking layers. Further, a heavily-doped *p*-type material was not known for transparent semiconductors even including *p*-type GaN. We like to introduce a series of layered oxychalcogenides that conform these requirements in Section 3.

It would be fair to note that ZnO will be an exception in the near future because it exhibits exctionic UV emission, and reliability, reproducibility and properties of *p*-type ZnO have been improved significantly in the few years [2, 3, 33]. However, emission properties are deteriorated in all the presently available *p*-type ZnO due to high-density acceptor doping. ZnO has another advantages because solid-solutions such as (Zn, Mg)O can be used for electron blocking layer, by which resonant tunneling diodes are fabricated and electron confinement effects are observed in ZnO/(Zn, Mg)O heterostructure devices [2, 4, 33–35]. Nevertheless, we still think it is important to seek new materials because we wonder if stability and controllability of carrier concentration in ZnO will be able to meet with the requirements of practical devices.

3 New *p*-type transparent semiconductor: Layered oxychalcogenides and excitonic blue LED

3.1 Optical and electronic properties

We have sought good *p*-type TOSs following our material exploration concept (see refs. [1, 6, 7, 36] for details). We

found that layered oxychalcogenides LaCuO*Ch* would be a new promising candidate because they offer various materials that have *p*-type conduction and excitonic light emission at room temperature. Mg-doped LaCuOSe exhibits degenerate *p*-type conduction with a conductivity of ∼ 140 S/cm [37], solid-solusion of LaCuO(S, Se, Te) provides a flexibility to tune their bandgap [38], and another similar material $La_2CdO_2Se_2$ may be used for intrinsic light-emitting layer and electron blocking layer [39]. It should be noted that their crystal structures, where (La_2O_2) layers and (Cu_2Ch_2) layers are alternately stacked (see Fig. 2(A) for LaCuOCh), are essentially important to understand the peculiar optoelectronic properties.

As noted above, LaCuO*Ch* exhibits good *p*-type conduction. For example, undoped LaCuOS have a hole concentration of $\sim 10^{19}$ cm^{-3} and Hall mobility of $\sim$0.5 cm^2(Vs)$^{-1}$ at room temperature. Mobility becomes larger with an increase in the Se content in LaCuO($S_{1-x}Se_x$) and reaches $\sim$ 8.0 cm^2(Vs)$^{-1}$ in LaCuOSe [37], which value is comparable to that of *p*-type GaN:Mg. Another important property of these materials is that degenerate *p*-type conduction is achieved in Mg-doped LaCuOSe, while undoped LaCuOSe shows thermally-activated behavior in hole concentration at around room temperature (Fig. 2(A)). This is the first degenerate *p*-type conductor for wide bandgap semiconductors even including *p*-type Mg-doped GaN.

From optical absorption spectra, we can see that LaCuOS is a transparent semiconductor having a bandgap about 3.3 eV (Fig. 2(B), measured at 10 K). The bandgap of LaCuOSe is smaller, but still large (∼2.9 eV). The optical absorption spectra also show another interesting feature: step-wise structures with sharp peaks just on the edges of the steps are observed [40]. Such structure is similar to those observed in semiconductor artificial superlattices [41], and would reflect two-dimensional density of states. The sharp peak features have been assigned to electron-hole pairs known as excitons from studies on photoluminescence (PL), optical nonlinear measurements and so on [42, 43]. It should be emphasized that the excitons are stable even at room temperature, which would be interesting because usually excitons are not so stable in solid inorganic semiconductors. Only ZnO is known to have room-temperature stable exctions in oxide semiconductors.

3.2 Electronic structure

As described above, layered oxychalcogenides exhibit interesting optoelectronic properties. Here, we discuss the origins of these properties based on their electronic structures. The first issue is easy to answer: the increase in the mobility with selenium content in LaCuO($S_{1-x}Se_x$) is explained by larger hybridization between Se and Cu than that between S and Cu, which increases the valence band (VB) widths and reduces the hole effective mass [37].

The next issue would be more interesting: it should be reminded that moderately large hole mobility of ∼4 cm^2/Vs and intense PL are maintained in the heavily doped LaCuOSe:Mg having a carrier concentration greater than 10^{20} cm^{-3} [40]. Usually, carrier mobility is significantly reduced by charged impurity scattering in such heavily-doped materials, but it is not the case in LaCuOSe. Similarly moderately intense excitonic PL is maintained in the heavily doped materials. It was shown from band structure calculations that the valence band dispersion of LaCuO*Ch* is much smaller in Γ-Z direction than in Γ-X direction, suggesting that the electronic structure is highly two-dimensional [40, 45]. Partial density-of-state analysis showed that the band gap is formed almost solely of the (Cu_2Ch_2) layers. The two-dimensional electronic structure is more clearly seen in the density map of holes in the vicinity of valence band maximum

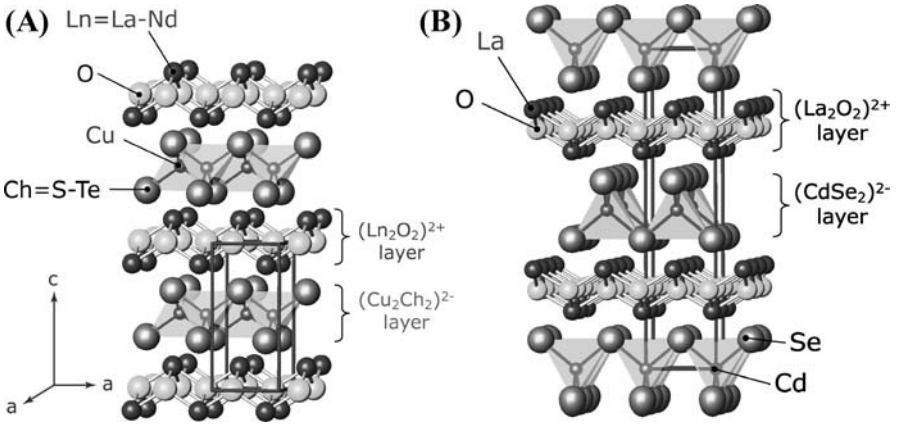

Fig. 1 Crystal structures of layered oxychalcogenides. (A) *Ln*CuO*Ch* (*Ln* = lanthanides, *Ch* = chalcogens). Alternate stacking of (Ln_2O_2) and (Cu_2Ch_2) layers forms the layered crystal structure. Edge-sharing network of CuCh_4 tetrahedra forms the (Cu_2Ch_2) layer. (B) $La_2CdO_2Se_2$. Alternate stacking of (La_2O_2) and $(CdSe_2)$ layers forms the layered crystal structure. The difference from *Ln*CuO*Ch* is that corner-sharing network of $CdSe_4$ tetrahedra forms the $(CdSe_2)$ layer

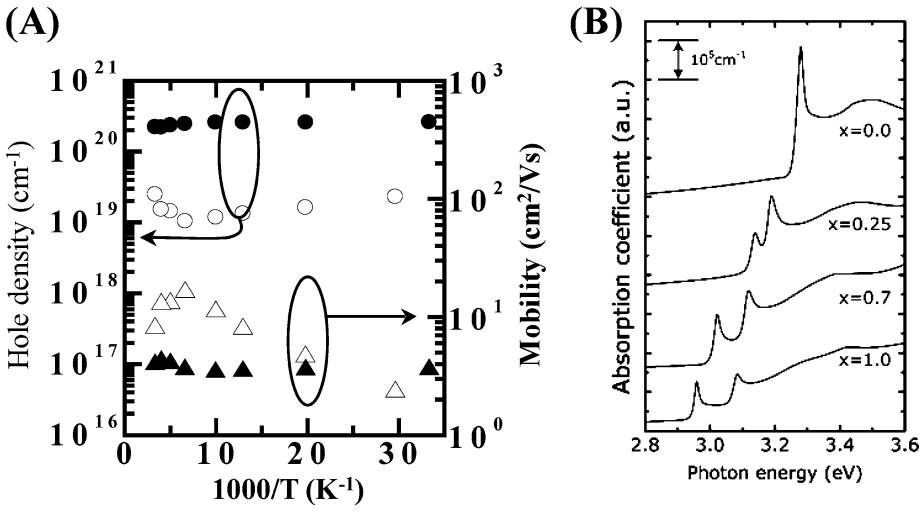

Fig. 2 Opto-electronic properties of $LaCuO(S_{1-x}Se_x)$. (A) Temperature dependence of Hall mobility and concentration of undoped (open symbols) and Mg-doped LaCuOSe (closed symbols). (B) Optical absorption spectra measured at 10 K for undoped $LaCuO(S_{1-x}Se_x)$

(VBM) in Fig. 3(A). Here, darker area has higher-density holes, showing that holes are confined in the (Cu_2Ch_2) layers, which forms the hole transport paths. Multiple sharp peak features in the optical absorption spectra shown in Fig. 2(B) is explained by multiple exciton levels split by spin-orbit interaction in *Ch* ions [40, 46]. This structure also explains why moderately large hole mobility is maintained in the heavily-doped LaCuOSe:Mg. In that case, Mg ions are doped in the LaO layers and generate holes. The generated holes are transferred to the (Cu_2Se_2) layer because of the local band offset (Fig. 3(B)). It consequently separates the charged acceptors and the mobile holes, and suppresses the charged impurity scattering, which is an analogue to modulation doping in high electron mobility transistors and semiconductor artificial superlattices.

The last issue is the wide bandgap of the layered oxychalcogenides. Simple chalcogenides, Cu_2S and Cu_2Se, have rather small bandgaps of ∼1.2–1.4 eV [47], but e.g. LaCuOS has much larger bandgap of ∼3.1 eV (at room temperature) although the bandgaps of Cu_2Ch and LnCuO*Ch* are mainly determined by the Cu*Ch* components. Electronic structure calculations also revealed the reason. It is possible to compare LaCuO*Ch* and Cu_2Ch, but we did not employ this approach because the comparison is not so clear due to different network structures of the $CuCh_4$ tetrahedra in these crystals. Therefore we employed a family compound with a similar crystal structure, $La_2CdO_2Se_2$ (crystal structure is shown in Fig. 1(B)), because its CdSe layer has a similar structure to that in CdSe. Figure 4 compares their band structures, showing that the VB width is not different largely, but the conduction band (CB) width is much smaller in $La_2CdO_2Se_2$. That means, the two-dimensional network structure of the CdSe layer reduces the CB dispersion and causes the large bandgap. It suggests that employing a low-dimensional structure is an effective approach to design new wide bandgap semiconductors. It was also confirmed that the reduction of CB dispersion is smaller in LaCuO*Ch* because $CuCh_4$ tetrahedra forms edge-sharing networks: however, similar qualitative explanation is still valid for the bandgap difference between LaCuO*Ch* and Cu_2Ch.

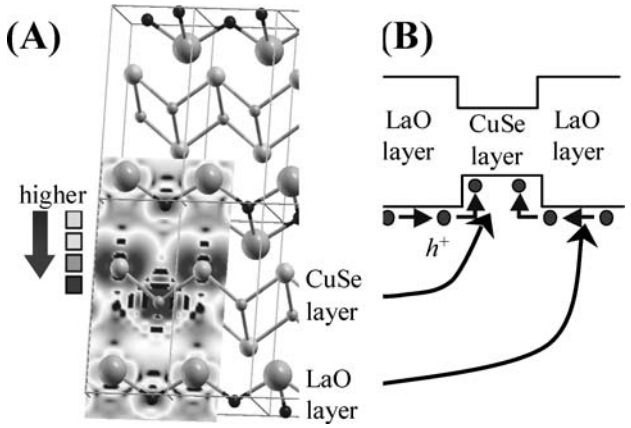

Fig. 3 Two-dimensional electronic structure in LnCuOSe. (A) Density map of valence top holes superimposed on the crystal structure. Darker area shows higher hole concentration. (B) Schematic illustration of simplified local electronic structure near the bandgap deduced from partial density of state analysis

3.3 Excitonic blue light-emitting diode

As a demonstration of a device application, we fabricated *p/n* junction structure LEDs using LaCuOSe for light-emitting *p*-layer (Fig. 5(A)). Amorphous indium gallium oxide (a-IGZO) was used for electron-injection n-layer. It exhibits sharp blue light emission originating from the exction in LaCuOSe at room temperature (B) [48].

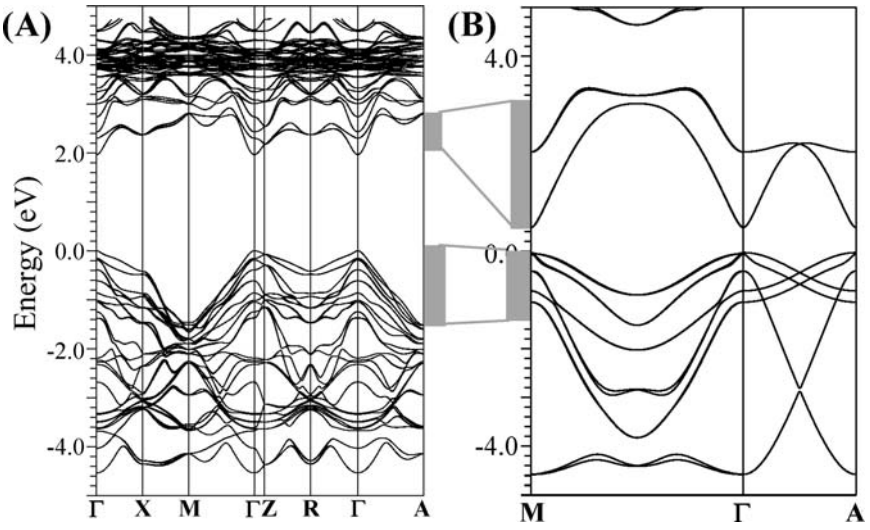

Fig. 4 Band structures of (A) $La_2CdO_2Se_2$ and (B) CdSe. The gray rectangles indicate CB and VB widths

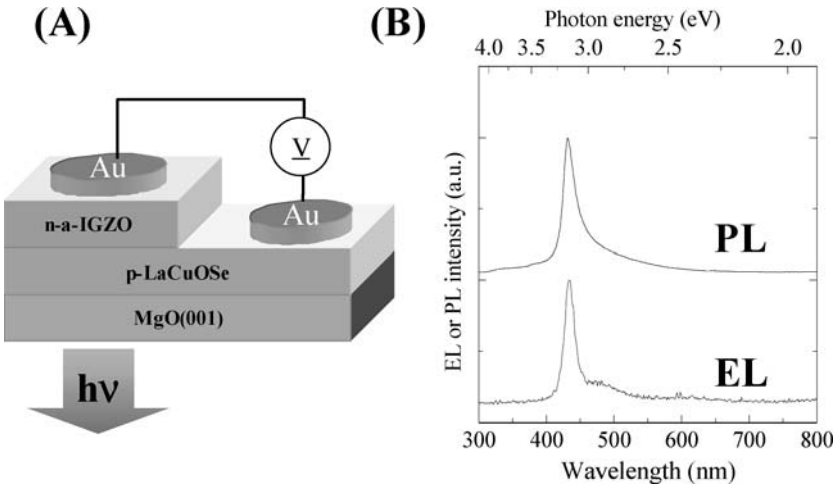

Fig. 5 (A) Structure of *p/n* junction LED and (B) PL and electroluminescence (EL) spectra at a current density of 1.9 Acm^{-2}

4 Amorphous oxide semiconductor: New semiconductor for giant-microelectronics

4.1 Requirements for flexible electronics

In Section 2, we introduced high-performance transparent TFTs using single-crystalline layers of $InGaO_3(ZnO)_5$ for channels. In spite of the good characteristics, it would not be applicable to practical applications because it needs very high process temperatures $>1300^{\circ}C$ to produce the single-crystalline layer [49, 50] and expensive single-crystalline substrates of yttria-stabilized zirconia (YSZ). Although it is possible to fabricate polycrystalline oxide TFTs using ZnO and $InGaO_3(ZnO)_m$ at low temperatures including room temperature [30, 31, 51, 52], here we like to propose that AOSs are promising for low-temperature processed applications.

Flexible electronics is expected to develop new devices, e.g. paper-like displays. Such devices have many requirements such as large-area uniform formation of more than millions devices, low-temperature fabrication on flexible substrates and so on. Hydrogenated amorphous silicon (a-Si:H) [26] and organic semiconductors have been examined for these purposes. However, the largest problem in these materials is the low carrier mobilities, only less than 1 cm^2/Vs, which limits their applications to low-speed or low-resolution display devices. As for an organic light-emitting diode (OLED), since it is operated by current injection to a light-emitting layer, driving transistors in OLED must have high current drivability. That means, TFTs in OLED must have a large channel width or large field-effect mobility. It is possible to employ high-mobility low-temperature polycrystalline silicon (LTPS) for TFTs [53]: however the distribution of device characteristics is not acceptable and an extra circuit using two or more transistors

must be integrated in each pixel for compensating the distribution of the TFT characteristics, which reduces an aperture ratio for bottom-emission OLEDs. In addition to these requirements, semiconductor materials have to be able to control carrier density at low concentrations, e.g. well below 10^{17} cm^{-3}, to control device characteristics [7].

4.2 Material exploration

From these viewpoints, we have sought AOSs [54, 55] with reasonably large mobilities and good controllability of carrier concentration. Here we show an example of our material exploration using an In_2O_3–ZnO–Ga_2O_3 system (detail will be published in refs. [56]). It was confirmed that amorphous films were formed at room temperature in the whole area of this system except for the areas near pure ZnO and In_2O_3. Hall mobilities greater than 10 $cm^2(Vs)^{-1}$ were obtained in the films having small Ga_2O_3 concentrations. We should be careful to interpret this data because previous study revealed that mobility in these materials systems increases with increasing carrier density [57, 58], and therefore it is thought that this result is associated more with the carrier concentration of the films. So we examined the relationship between mobility and carrier concentration at room temperature for AOSs with nominal compositions of $In_2Zn_3O_7$ (a-IZO) and $InGaZnO_4$ (a-IGZO) (Fig. 6(A)). It is seen that although both the materials have mobilities larger than 10 cm^2/Vs, a-IZO looks better. However, it is more difficult for a-IZO to suppress the carrier concentration down to well below 10^{17} cm^{-3} (B). Even if the initial carrier concentration is suppressed by further increasing the oxygen partial pressure during film deposition, it was not stable and the electrical conductivity recovered to the large values.

4.3 Thin film transistors

We fabricated TFTs using a-IZO for channels at room temperature. But on-off current ratios were only one order of magnitude for most of the devices, which is thought to reflect the large conductivity (i.e. high carrier concentrations) of the a-IZO channels. It is possible to reduce the off current in a-IZO TFTs by further optimization. In this case, we unexpectedly obtained abnormally large apparent field effect mobilities greater than 100 cm^2/Vs (Fig. 7(A)). However, in such cases a large threshold voltage shift was observed in the hysteresis curve, thus the large mobility value is not likely the intrinsic performance of the device.

Therefore, we finally chose a-IGZO from the viewpoints of controllability and stability of carrier concentration. Carrier concentration can be controlled at low values less than 10^{15} cm^{-3} in a-IGZO films. In addition, it was also confirmed that a-IGZO forms a very stable amorphous phase up to 500°C. Then we fabricated TFTs using a-IGZO for channels at room temperature. Their characteristics were stable for more than 10 repetition measurements, and only very small hysteresis was observed with reasonable field effect mobilities of ~6.5 cm^2/Vs (B). We also fabricated transparent TFTs on plastic (PET) substrates at room temperature using ITO for electrodes. The devices exhibited a large mobility for flexible TFTs, about 8 cm^2/Vs [59]. Even after a bending test, they worked with similar characteristics: only small decrease in mobility to 7 cm^2/Vs was observed. It was stable for several bending tests after the first bending. Recently some improvement has been made in device characteristics, and mobilities

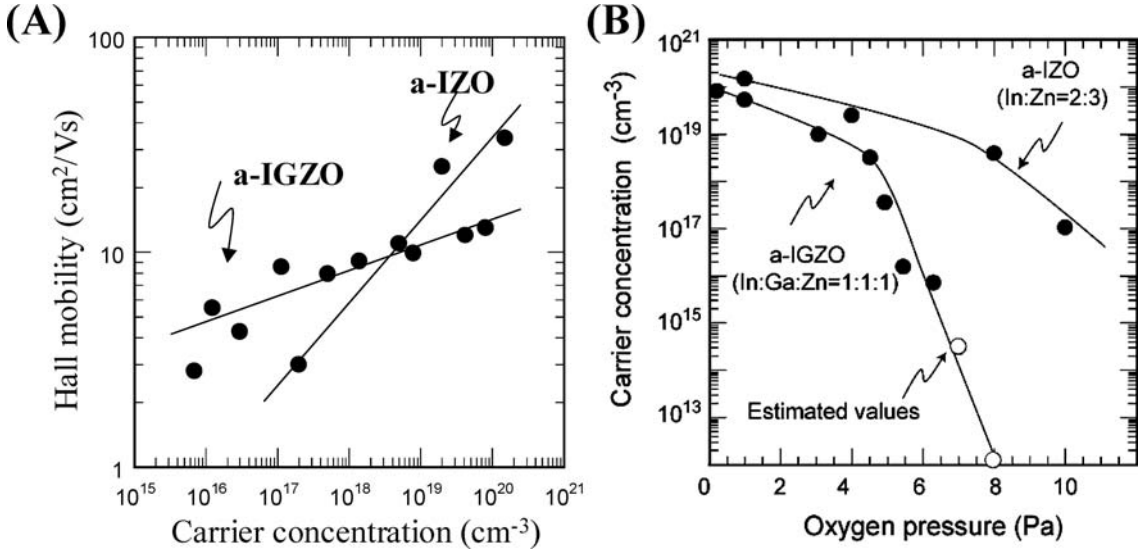

Fig. 6 Carrier transport properties of a-IZO and a-IGZO. (A) Relationship between room-temperature Hall mobility and carrier concentration. (B) Carrier concentration as a function of oxygen pressure during film deposition

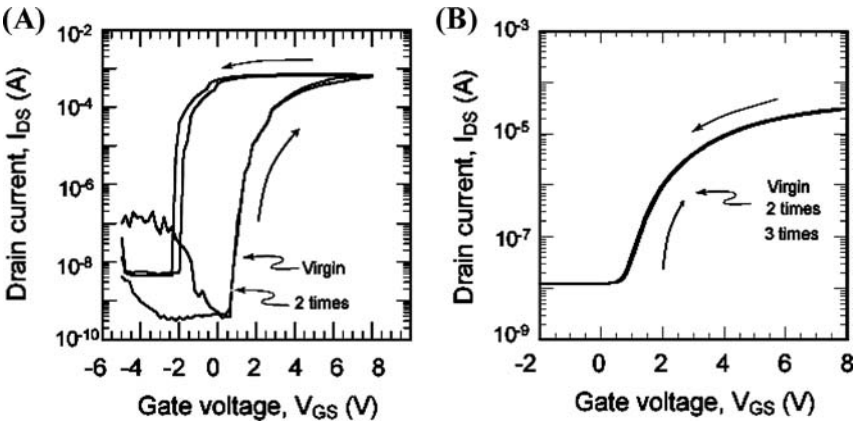

Fig. 7 (A) Transfer characteristic of a-IZO TFT exhibiting an apparent field effect mobility of ∼100 $cm^2(Vs)^{-1}$. It shows large hysteresis (measured at a gate voltage scanning speed of 2 V/s). (B) Transfer characteristic of a-IGZO TFT exhibiting a field effect mobility of ∼6.5 $cm^2(Vs)^{-1}$. Its hysteresis is negligibly small (measured at 5 V/s)

greater than 10 cm^2/Vs and on-off current ratios $\sim 10^6$ are reproducibly available.

4.4 Carrier transport: Difference between AOS and a-Si:H

As well known, a-Si:H is another candidate for low-temperature device applications. We have found that there are many and large differences between AOS and a-Si:H, which becomes clearer if comparing them with associated crystalline phases. We have observed that the carrier transport properties of crystalline (sc-) and amorphous (a-) IGZO are similar although their structures are completely different [56, 59]. For example, in both the materials, mobility increases with the increasing electron density, and exceeds 10 cm^2/Vs at high electron concentrations [57, 58]. By contrast, intrinsic crystalline silicon has a large electron mobility of ∼1500 cm^2/Vs, but the mobility is reduced to only $<\sim 1$ cm^2/Vs in a-Si:H. It was also found that tail-like states are formed around the conduction band bottom (i.e. below and above the mobility edge) in sc-IGZO and a-IGZO. The tail-like states are not localized and have exponential decay with energy widths of only 25 meV for sc-IGZO and 6 meV for a-IGZO. In a-Si:H, its tail-state also has an exponential decay similar to IGZO. But it is located below the mobility edge and localized. The energy width in device-grade a-Si:H is ∼ 45 meV, which is rather larger than that in IGZO have. Degenerate conduction and large mobilities >10 $cm^2(Vs)^{-1}$ are easily attained in a-IGZO. In addition, it works as semiconductor even if it is formed at room temperature without any defect passivation. While, in a-Si:H, degenerate conduction has never been achieved, mobility is low, $<\sim 1$ $cm^2(Vs)^{-1}$, and hydrogen passivation is necessary to be used for optoelectronic applications [26]. It is reported that the electrical conductivity can run up only to 0.1 S/cm, and the activation energies are leveled off around 0.2 eV because higher doping has never been achieved.

The similar carrier transport in crystalline and amorphous oxides is qualitatively understood by considering carrier transport paths [54]. In silicon, carrier transport paths are formed by sp^3 hybridized orbitals. It forms periodic regular network in perfect crystals and carriers can flow with the large mobility of ∼1500 $cm^2(Vs)^{-1}$. However, in a disordered amorphous structure, the overlapping between the adjacent sp^3 orbitals varies largely because sp^3 orbitals have strong spatial directivity. It forms rather deep and high-density localized tail states. Consequently it causes hopping conduction and low mobility ($<\sim 1$ $cm^2(Vs)^{-1}$) in a-Si:H. In oxides, the electron transport paths are formed by spherical s oribitals of metal cations. So the overlapping between the adjacent s orbitals is not affected largely by the disordered amorphous structure. Therefore, transport properties in amorphous phase would be similar to those in crystalline phase in oxides.

A simple electronic model would also explain the difference in the passivation behavior. In Si, bonding and antibonding sp^3 hybridized orbitals form VB maximum (VBM) and CB minimum (CBM), respectively (Fig. 8(A)). Therefore if a silicon vacancy is formed, the neighboring Si atom forms a non-bonding level (dangling bond) near the middle of the bandgap (B). If such deep levels are formed at a high density in the bandgap, the Fermi level can not be altered by impurity doping and external electric field anymore; therefore such material does not work as semiconductor. Formation of Si-H bonds pushes the dangling bond levels out into the CB and VB (hydrogen passivation) (C). By contrast, in oxides, if an oxygen vacancy is formed, the non-bonding state of a metal cation can be in the CB or close to CBM in some oxides. In such case, no deep level is formed and passivation is not necessary. It should be noted that real situation is not so simple and structural relaxation should be considered [7, 60]. If an occupied level is located at a high energy as illustrated in (E), its energy level is lowered significantly by structural relaxation and is possible to be placed even at energy close to VBM as illustrated in (F). Similar relaxation

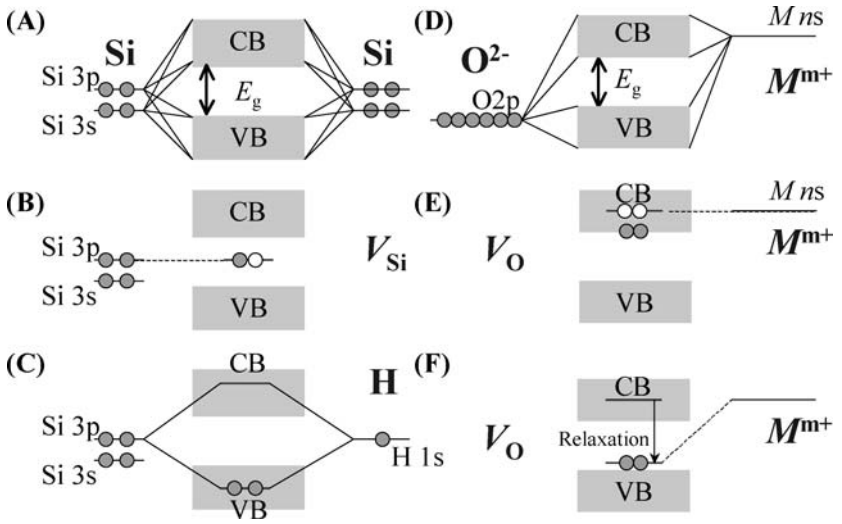

Fig. 8 Schematic illustration of simplified electronic structures of silicon (A–C) and oxides (D–F). Open circles show unoccupied states and closed circles occupied states. (A) Perfect Si crystal. (B) A Si vacancy is formed. A dangling bond level is formed around the middle of the bandgap. (C) The dangling bond is passivated by H. (D) Perfect oxide crystal. (E) An oxygen vacancy is formed. A metal non-bonding state may remain in CB or near CBM if no structural relaxation occurs. No in-gap state is formed and electrons released from the oxygen vacancy work as mobile carriers in CB. In this case, no passivation is needed. (F) More care should be paid to the other (and probably many) cases. Metal non-bonding states are much lowered into the band gap due to local structural relaxation around the oxygen vacancy. In this case, the mobile carriers are annihilated, but again no trapping state is formed in the bandgap if the Fermi level is higher than the relaxed oxygen vacancy state and the relaxed defect level is fully occupied

of a defect structure is known as color center in wide bandgap materials such as alkali halides and alkali-earth oxides [60]. Recent works on ZnO have suggested that neutral oxygen vacancies also forms very deep levels close to VBM (note that it may need further study to make a final conclusion) [61, 62]. Even in such a case, if the relaxed level is lower than the Fermi level, the fully occupied centers do not work as trapping centers, and therefore no passivation is needed.

5 Summary

We have explored new transparent oxide semiconductors and fabricated devices utilizing unique features inherent to these materials. In this review, we described requirements for active layer materials in practical devices and our strategy for material exploration based on consideration of electronic structures. Two new materials, layered oxychalcogenides and amorphous oxide semiconductors, were shown as examples. We like to note that oxides can have many advantages over conventional materials and devices if we find suitable applications. If we limit an application to low-temperature devices, amorphous oxides have many advantages, such as a large mobility, a simple device process without passivation, and transparency. If we intend to develop optoelectronic devices in short wavelength region, oxide-based wide bandgap semiconductors, such as LaCuO*Ch* and Ga_2O_3, may be promising candidates. In addition, use of low-dimensional or nano-structures naturally formed in oxides would provide flexibility for simultaneous control of multiple properties as described in Section 3.2 e.g. for rendering good *p*-type conduction and wide bandgap in layered oxychalcogenides.

References

1. H. Kawazoe, M. Yasukawa, H. Hyodo, M. Kurita, H. Yanagi, and H. Hosono, *Nature*, **389**, 939 (1997).
2. A. Ohtomo and A. Tsukazaki, *Semicond. Sci. Technol.*, **20**, S1 (2005).
3. D.C. Look, *Semicond. Sci. Technol.*, **20**, S55 (2005).
4. T. Makino, Y. Segawa, M. Kawasaki, and H. Koinuma, *Semicond. Sci. Technol.*, **20**, S78 (2005).
5. Y. Tokura, *Physics Today*, **50** (2003).
6. H. Hosono, T. Kamiya, and M. Hirano, *Bull. Chem. Soc. Jpn.*, **79**, 1 (2006).
7. T. Kamiya and H. Hosono, *Semicond. Sci. Technol.*, **20**, S92 (2005).
8. H. Hosono, *Int. J. Appl. Ceram. Technol*, **1**, 106 (2004).
9. H. Ohta and H. Hosono, *Materials Today*, **Jun**, 42 (2004).
10. H. Ohta, K. Kawamura, M. Orita, M. Hirano, N. Sarukura, and H. Hosono, *Appl. Phys. Lett.*, **77**, 475 (2000).
11. H. Ohta, M. Orita, M. Hirano, and H. Hosono, *J. Appl. Phys.*, **89**, 5720 (2001).
12. K. Nomura, H. Ohta, K. Ueda, T. Kamiya, M. Hirano, and H. Hosono, *Science*, **300**, 1269 (2003).
13. M. Orita, H. Ohta, M. Hirano, and H. Hosono, *Appl. Phys. Lett.*, **77**, 4166 (2000).
14. M. Orita, H. Hiramatsu, H. Ohta, M. Hirano, and H. Hosono, *Thin Solid Films*, **411**, 134 (2002).
15. K. Matsuzaki, H. Yanagi, T. Kamiya, H. Hiramatsu, K. Nomura, M. Hirano, and H. Hosono, *Appl. Phys. Lett.*, **88**, 092106 (2006).
16. M. Oto, S. Kikugawa, N. Sarukura, M. Hirano, and H. Hosono, *IEEE Photon. Technol. Lett.*, **13**, 978 (2001).

17. M. Oto, S. Kikugawa, T. Miura, M. Hirano, and H. Hosono, *J. Non-Cryst. Sol.,* **349**, 133 (2004).
18. K. Hayashi, M. Hirano, S. Matsuishi, and H. Hosono, *J. Am. Chem. Soc.*, **124**, 738 (2002).
19. K. Hayashi, S. Matsuishi, T. Kamiya, M. Hirano, and H. Hosono, *Nature*, **419**, 462 (2002).
20. S. Matsuishi, Y. Toda, M. Miyakawa, K. Hayashi, T. Kamiya, M. Hirano, I. Tanaka, and H. Hosono, *Science*, **301**, 626 (2003).
21. Y. Toda, S. Matsuishi, K. Hayashi, K. Ueda, T. Kamiya, M. Hirano, and H. Hosono, *Adv. Mater.*, **16**, 685 (2004).
22. Y. Toda, S.W. Kim, K. Hayashi, M. Hirano, T. Kamiya, H. Hosono, T. Haraguchi, and H. Yasuda, *Appl. Phys. Lett.*, **87**, 254103 (2005).
23. T. Kamiya, S. Aiba, M. Miyakawa, K. Nomura, S. Matsuishi, K. Hayashi, K. Ueda, M. Hirano, and H. Hosono, *Chem. Mater.*, **17**, 6311 (2005).
24. T. Kamiya and H. Hosono, *Jpn. J. Appl. Phys.*, **44**, 774 (2005).
25. T. Kamiya, H. Ohta, H. Hiramatsu, K. Hayashi, K. Nomura, S. Matsuishi, K. Ueda, M. Hirano, and H. Hosono, *Microelectr. Eng.*, **73–74**, 620 (2004).
26. W.E. Spear and P.G. LeComber, *Solid State Commun.*, **17**, 1193 (1975).
27. W.E. Spear, G. Willeke, and P.G. LeComber, *Physica B*, **117–118**, 908 (1983).
28. S. Narushima, K. Ueda, H. Mizoguchi, H. Ohta, M. Hirano, K. Shimizu, T. Kamiya, and H. Hosono, *Adv. Mater.*, **15**, 1409 (2003).
29. T. Kamiya, S. Narushima, H. Mizoguchi, K. Shimizu, K. Ueda, H. Ohta, M. Hirano, and H. Hosono, *Adv. Funct. Mater.*, **15**, 968 (2005).
30. E.M.C. Fortunato, P.M.C. Barquinha, A.C.M.B.G. Pimentel, A.M.F. Gonçalves, A.J.S. Marques, R.F.P. Martins, and L.M.N. Pereira, *Appl. Phys. Lett.*, **85**, 2541 (2004).
31. E.M.C. Fortunato, P.M.C. Barquinha, A.C.M.B.G. Pimentel, A.M.F. Concalves, A.J.S. Marques, L.M.N. Perera, and R.F.P. Martins, *Adv. Mater.*, **17**, 590 (2005).
32. H. Hosono, *J. Cryst. Growth*, **237–239**, 496 (2002).
33. A. Tsukazaki, A. Ohtomo, T. Onuma, M. Ohtani, T. Makino, M. Sumiya, K. Ohtani, Su.F. Chichibu, S. Fuke, Y. Segawa, H. Ohno, H. Koinuma, and M. Kawasak, *Nature Mater.*, **4**, 42 (2004).
34. S. Krishnamoorthy, A.A. Iliadis, A. Inumpudi, S. Choopun, R.D. Vispute, and T. Venkatesan, *Sol. Stat. Electr.*, **46**, 1633 (2002).
35. T. Edahiro, N. Fujimura, and T. Ito, *J. Appl. Phys.*, **93**, 7673 (2003).
36. K. Ueda, K. Takafuji, H. Hiramatsu, H. Ohta, M. Hirano, H. Hosono, and H. Kawazoe, *Mater. Res. Soc. Symp. Proc.*, **747**, 223 (2003).
37. H. Hiramatsu, K. Ueda, H. Ohta, M. Hirano, T. Kamiya, and H. Hosono, *Appl. Phys. Lett.*, **82**, 1048 (2003).
38. H. Hiramatsu, K. Ueda, K. Takafuji, H. Ohta, M. Hirano, T. Kamiya, and H. Hosono, *J. Appl. Phys.*, **94**, 5805 (2003).
39. H. Hiramatsu, K. Ueda, T. Kamiya, H. Ohta, M. Hirano, and H. Hosono, *J. Phys. Chem. B*, **108**, 17344 (2004).
40. K. Ueda, H. Hiramatsu, H. Ohta, M. Hirano, T. Kamiya, and H. Hosono, *Phys. Rev. B*, **69**, 155305 (2004).
41. e.g., A. Shink, *Quantum Wells* (World Scientific, Singapore, 1997).
42. H. Kamioka, H. Hiramatsu, H. Ohta, M. Hirano, K. Ueda, T. Kamiya, and H. Hosono, *Appl. Phys. Lett.*, **84**, 879 (2004).
43. H. Kamioka, H. Hiramatsu, M. Hirano, K. Ueda, T. Kamiya, and H. Hosono, *Opt. Lett.*, **29**, 1659 (2004).
44. H. Hiramatsu, K. Ueda, H. Ohta, M. Hirano, T. Kamiya, and H. Hosono, *Thin Solid Films*, **445**, 304 (2003).
45. S. Inoue, K. Ueda, and H. Hosono, *Phys. Rev. B*, **64**, 245211 (2001).
46. T. Kamiya, K. Ueda, H. Hiramatsu, H. Kamioka, H. Ohta, M. Hirano, and H. Hosono, *Thin Solid Films*, **486**, 98 (2005).
47. *Semiconductors: Data Handbook*, 3rd edn., (Springer), pp. 454–457, (ISBN 3-540-40488-0).
48. H. Hiramatsu, K. Ueda, H. Ohta, T. Kamiya, M. Hirano, and H. Hosono, *Appl. Phys. Lett.*, **87**, 211107 (2005).
49. H. Ohta, K. Nomura, M. Orita, M. Hirano, K. Ueda, T. Suzuki, Y. Ikuhara, and H. Hosono, *Adv. Funct. Mater.*, **13**, 139 (2003).
50. K. Nomura, H. Ohta, T. Suzuki, C. Honjyo, K. Ueda, T. Kamiya, M. Orita, Y. Ikuhara, M. Hirano, and H. Hosono, *J. Appl. Phys.*, **95**, 5532 (2004).
51. S. Masuda, K. Kitamura, Y. Okumura, S. Miyatake, H. Tabata, and T. Kawai, *J. Appl. Phys.*, **93**, 1624 (2003).
52. J. Nishii, F.M. Hossain, S. Takagi, T. Aita, K. Saikusa, Y. Ohmaki, I. Ohkubo, S. Kishimoto, A. Ohtomo, T. Fukumura, F. Matsukura, Y. Ohno, H. Koinuma, H. Ohno, and M. Kawasaki, *Jpn. J. Appl. Phys.*, **42**, L347 (2003).
53. T. Sameshima, *J. Non-Cryst. Solids*, **227–230**, 1196 (1998).
54. H. Hosono, N. Kikuchi, N. Ueda, and H. Kawazoe, *J. Non-Cryst. Solids*, **198–200**, 165 (1996).
55. H. Hosono, M. Yasukawa, and H. Kawazoe, *J. Non-Cryst. Solids*, **203**, 334 (1996).
56. K. Nomura, A. Takagi, T. Kamiya, H. Ohta, M. Hirano, and H. Hosono, *Jpn. J. Appl. Phys.*, (2005) in print.
57. K. Nomura, H. Ohta, K. Ueda, T. Kamiya, M. Hirano, and H. Hosono, *Appl. Phys. Lett.*, **85**, 1993 (2004).
58. A. Takagi, K. Nomura, H. Ohta, H. Yanagi, T. Kamiya, M. Hirano, and H. Hosono, *Thin Solid Films*, **486**, 38 (2005).
59. K. Nomura, H. Ohta, A. Takagi, T. Kamiya, M. Hirano, and H. Hosono, *Nature*, **432**, 488 (2004).
60. F. Agullo-Lopez, C.R.A. Catlow, and P.D. Townsend, *Point Defects in Materials* (Academic Press, London, 1988).
61. A.F. Kohan, G. Ceder, D. Morgan, and C.G.V. Walle, *Phys. Rev. B*, **61**, 15019 (2000).
62. F. Oba, S.R. Nishitani, S. Isotani, H. Adachi, and I. Tanaka, *J. Appl. Phys*., **90**, 824 (2001).